A Consensus-Based Control Law for Accurate Frequency Restoration and Power Sharing in Microgrids in the Presence of Clock Drifts*

Ajay Krishna[1], Johannes Schiffer[2] and Jörg Raisch[1,3]

***Abstract*— Clock drifts are a common phenomenon in distributed systems, such as microgrids (MGs). Unfortunately, if not accounted for, the presence of clock drifts can hamper accurate frequency restoration and power sharing in MGs. As a consequence, we have proposed in [1] a distributed secondary frequency control that ensures an accurate stationary control performance in the presence of clock drifts. In the present work, we extend the analysis in [1] by providing a tuning criterion for the controller parameters that guarantees robust stability of a given equilibrium point of the closed-loop dynamics with respect to uncertain bounded clock drifts. Finally, our analysis is validated on an exemplary MG via simulation.**

I. Introduction

Electric power systems (PSs) around the globe are currently facing new changes and challenges which are mainly due to the increasing presence of renewable energy sources (RESs). At present, the electric PS contains a large number of small units rather than a small number of large power stations. These small units are usually equipped with RESs. The volatile and intermittent nature of RESs increase uncertainties in the grid. To interface RESs into the electric grid, power electronic inverters are used. Furthermore, the physical characteristics of inverters largely differ from the characteristics of conventional generators. Therefore, new and intelligent control concepts which ensure stable and reliable PS operation are needed. In this context, the concept of MGs is foreseen as a promising solution [2]. A MG is a locally controllable subset of a large PS. It consists of several RESs, storage units and corresponding loads. MGs can typically work in islanded or grid-tied mode [2]. In this paper, we are interested in the former case.

As in any AC power system, frequency stability is a key performance criterion in MGs. In inverter-dominated MGs, so-called grid forming inverters (GFIs) are employed for this task. A GFI is a voltage source inverter which is controlled using pre-defined voltage and frequency values [2], see [3] for further details on modeling of MGs. Inspired by conventional power systems, a hierarchical control strategy is advocated in case of MGs [4]. The primary control layer consists of a decentralized proportional control, called *droop control*, which guarantees stability and power sharing [5]. Droop control achieves its control objectives at the expense of steady state deviation in frequency and voltage, which in general is tackled using a centralized integral secondary control [4]. However, considering the increasing complexity in network dynamics together with the distributed nature of power generation and consumption in MGs, distributed secondary control architectures are more appealing [6]. Finally, the third control layer called the energy management deals with generation scheduling [4].

In this paper, we are interested in distributed secondary frequency control in MGs which uses local information as well as neighboring information over a communication network to ensure frequency restoration and power sharing. In an inverter-dominated MG, each inverter typically has only a local understanding of time, which leads to clock inaccuracies [7]. In practice, clock drifts [8] are non-negligible phenomena in distributed MG control [1]. Hence, in the presence of clock drifts, internal frequencies of inverters are slightly different [9], [7]. Note that internal frequencies of inverters are employed in designing a distributed secondary frequency control [1]. However, most of the work on distributed secondary frequency control does not consider the effect of clock drifts. See for example, the *pinning control* scheme in [6], the distributed averaging integral (DAI) control in [10], [11], [12], [13]. We have shown in [1] that the presence of clock drifts impairs accurate frequency restoration and power sharing with the usual secondary control schemes. In [1], we use conventional frequency droop control at the primary control layer. Moreover, in [1], we have proposed an alternative secondary control law, termed generalized distributed averaging integral (GDAI) control, and provided a parametrization of the control parameters, such that the synchronized electrical frequency is the nominal frequency and, in addition, power sharing is ensured. In [14], an angle droop control, with consensus based frequency and power control to ensure power sharing in the presence of clock drifts is proposed. Note that the complete knowledge of phase angles to implement such an angle droop control in a MG is a restrictive assumption in practice.

In this paper, we extend the work in [1] by providing a design criterion in the form of a set of linear matrix inequalities (LMIs) which ensures that the GDAI control renders the equilibrium of the closed-loop system asymptotically stable (AS) in the presence of clock drifts and guarantees accurate frequency restoration and power sharing. Unlike in [14], we do not linearize the electrical network, instead we work with the non-linear MG model. Moreover, our design criterion

*The project leading to this manuscript has received funding from the German Academic Exchange Service (DAAD) and the European Union's Horizon 2020 research and innovation programme under the Marie Skłodowska-Curie grant agreement No. 734832.

[1]Fachgebiet Regelungssysteme, Technische Universität Berlin, Germany, {krishna, raisch}@control.tu-berlin.de

[2]School of Electronic and Electrical Engineering, University of Leeds, UK, j.schiffer@leeds.ac.uk

[3]Max-Planck-Institut für Dynamik komplexer technischer Systeme, Magdeburg, Germany

does not require knowledge of the operating point. We use a Lyapunov function with classic kinetic and potential energy terms to derive the design criterion. For a comprehensive analysis of the use of energy functions in the context of MGs, the reader is referred to [15]. Finally, we illustrate via simulation that with our design criterion, the GDAI controller achieves accurate frequency restoration, power sharing and local AS.

The paper is organized as follows. In Section II, we recall some preliminaries of graph theory, introduce the MG model and the GDAI control. In Section III, the design criterion for the closed loop system in the presence of clock drifts is presented. In Section IV, the design criterion is solved numerically and the results are simulated for an exemplary MG. Finally, we summarize our work and suggest some future research directions in Section V.

II. Preliminaries

We denote by I_n the $n \times n$ identity matrix, by $\mathbb{0}_{n\times m}$ the $n \times m$ matrix with all entries equal to zero, by $\mathbb{1}_n$ the vector with all entries being equal to one and by $\mathbb{0}_n$ the zero vector. The maximum eigenvalue of a square symmetric matrix F is denoted by $\lambda_{\max}(F)$. If F is positive (negative) definite, we denote this by $F > 0$ ($F < 0$). If F is positive (negative) semidefinite, we denote this by $F \geq 0$ ($F \leq 0$). Moreover, $A > B$ means that $A - B > 0$. Let $x = \text{col}(x_i)$ denote a vector with entries x_i, $Y = \text{diag}(y_i)$ a diagonal matrix with diagonal entries y_i and $X = \text{blkdiag}(X_i)$ a block-diagonal matrix with block-diagonal matrix entries X_i. Finally, $*$ denotes the elements below the diagonal of a symmetric matrix.

A. Algebraic graph theory

A weighted undirected graph of order $n > 1$ is a triple $\mathcal{G} = (\mathcal{N}, \mathcal{E}, \mathcal{W})$ with set of vertices $\mathcal{N} = \{1, \dots, n\}$. Furthermore, $\mathcal{E} \subseteq [\mathcal{N}]^2$ is the set of edges, where $[\mathcal{N}]^2$ represents the set of all two-element subsets of $\mathcal{N}$ and $\mathcal{W} : \mathcal{E} \to \mathbb{R}_{>0}$ is a weight function. The entries of the adjacency matrix $\mathcal{A} \in \mathbb{R}^{n\times n}$ of $\mathcal{G}$ are $a_{ij} = a_{ji} = w_l > 0$ if $\{i, j\} \in \mathcal{E}$ where $w_l = w(i, j) = w(j, i)$ is the edge weight and $a_{ij} = a_{ji} = 0$ otherwise. The set of neighboring nodes of node i is given by $\mathcal{N}_i = \{j \in \mathcal{N} \,|\, a_{ij} \neq 0\}$. The diagonal degree matrix $\mathcal{D} \in \mathbb{R}^{n\times n}$ is given by $\mathcal{D} = \text{diag}\big(\sum_{j\in\mathcal{N}} a_{ij}\big)$. A path is an ordered sequence of nodes such that any pair of consecutive nodes in the sequence is connected by an edge. The graph $\mathcal{G}$ is called connected if there exists a path between every pair of distinct nodes. The Laplacian matrix $\mathcal{L} \in \mathbb{R}^{n\times n}$ of an undirected graph is given by $\mathcal{L} = \mathcal{D} - \mathcal{A}$. The Laplacian matrix $\mathcal{L}$ is symmetric and positive semi-definite. If and only if $\mathcal{G}$ is connected, $\mathcal{L}$ has a simple zero eigenvalue. Then, a corresponding right eigenvector is $\mathbb{1}_n$, i.e., $\mathcal{L}\mathbb{1}_n = \mathbb{0}_n$. We refer the reader to [16], [17] for more information on graph theory.

B. Primary-controlled MG model with clock drifts

We consider a Kron-reduced representation [18] of an inverter-based MG and denote its set of network nodes by $\mathcal{N} = \{1, ..., n\}$, $n > 1$. The phase angle and voltage magnitude at each bus $i \in \mathcal{N}$ are denoted by $\delta_i : \mathbb{R}_{\geq 0} \to \mathbb{R}$, respectively, $V_i : \mathbb{R}_{\geq 0} \to \mathbb{R}_{>0}$. The electrical frequency at the i-th node is denoted by $\omega_i = \dot{\delta}_i$. As customary in secondary frequency control design, we assume that all voltage amplitudes are constant and that the line admittances are purely inductive [18], [19], [11]. The latter assumption is generally satisfied for MGs in which the inductive output impedance of the converter filter and/or transformer dominates the resistive part of the line impedances [5] and we only consider such MGs. Thus, if there is a power line between nodes $i \in \mathcal{N}$ and $k \in \mathcal{N}$, then this is represented by a nonzero susceptance $B_{ik} \in \mathbb{R}_{<0}$. Furthermore, the electrical network is assumed to be connected and the set of neighboring nodes of the i-th node is denoted by $\mathcal{N}_i = \{k \in \mathcal{N} \,|\, B_{ik} \neq 0\}$.

Following [9], [7], we denote by $\mu_i \in \mathbb{R}$ the constant relative drift of the clock of the i-th unit, $i \in \mathcal{N}$. In general, $|\mu_i| \ll 1$ is a small unknown parameter [9], [7]. Furthermore, it is convenient to introduce the *internal* frequency $\bar{\omega}_i : \mathbb{R}_{\geq 0} \to \mathbb{R}$ of the inverter at the i-th node which—under the assumption of sufficiently fast sampling times—yields the following relation between the *internal* frequency $\bar{\omega}_i$ and the *electrical* frequency ω_i:

$$\bar{\omega}_i = (1 + \mu_i)\omega_i, \quad i \in \mathcal{N}, \tag{II.1}$$

see [9], [7] for details. In the sequel, we refer to $\mu_i \in \mathbb{R}$ as the clock drift factor or simply clock drift.

Following standard practice, we assume that all units are equipped with the usual primary frequency droop control [4]. Then the dynamics of the generation unit at the i-th node, $i \in \mathcal{N}$, is given by

$$\begin{aligned} (1 + \mu_i)\dot{\delta}_i &= (1 + \mu_i)\omega_i = \bar{\omega}_i, \\ (1 + \mu_i)M_i\dot{\bar{\omega}}_i &= -D_i(\bar{\omega}_i - \omega^d) + P_i^d - G_{ii}V_i^2 + u_i - P_i, \end{aligned} \tag{II.2}$$

where $\omega^d \in \mathbb{R}$ is the desired electrical frequency, $P_i^d \in \mathbb{R}$ is the desired active power set point, $G_{ii}V_i^2 \in \mathbb{R}_{\geq 0}$ represents the constant power load at the i-th node, $D_i \in \mathbb{R}_{>0}$ is the inverse droop coefficient and $M_i = \tau_{P_i} D_i$ is the virtual inertia coefficient, where $\tau_{P_i} \in \mathbb{R}_{>0}$ is the time constant of the low pass filter for the power measurement [20]. Furthermore, $u_i : \mathbb{R}_{\geq 0} \to \mathbb{R}$ is the secondary control input. The active power flow $P_i : \mathbb{R}^n \to \mathbb{R}$ at the i-th node is given by[1]

$$P_i = \sum\nolimits_{k\in\mathcal{N}_i} |B_{ik}|V_iV_k \sin(\delta_i - \delta_k). \tag{II.3}$$

To derive a compact model representation of the MG, it is convenient to introduce the matrices

$$\begin{aligned} &D = \text{diag}(D_i) \in \mathbb{R}_{>0}^{n\times n}, M = \text{diag}(M_i) \in \mathbb{R}_{>0}^{n\times n}, \\ &\mu = \text{diag}(\mu_i) \in \mathbb{R}^{n\times n}, \end{aligned}$$

and the vectors

$$\begin{aligned} &\delta = \text{col}(\delta_i) \in \mathbb{R}^n, \omega = \text{col}(\omega_i) \in \mathbb{R}^n, \bar{\omega} = \text{col}(\bar{\omega}_i) \in \mathbb{R}^n, \\ &P^{\text{net}} = \text{col}(P_i^d - G_{ii}V_i^2) \in \mathbb{R}^n, u = \text{col}(u_i) \in \mathbb{R}^n. \end{aligned}$$

[1]For notational simplicity, time arguments of all signals are omitted.

Also, we introduce the *potential function* $U : \mathbb{R}^n \to \mathbb{R}$,

$$U(\delta) = -\sum\nolimits_{\{i,k\}\in[\mathcal{N}]^2} |B_{ik}|V_iV_k\cos(\delta_i - \delta_k).$$

Then, the dynamics (II.2), $\forall i \in \mathcal{N}$, can be compactly written as

$$\begin{aligned}(I_n + \mu)\dot{\delta} &= \bar{\omega},\\ (I_n + \mu)M\dot{\bar{\omega}} &= -D(\bar{\omega} - \mathbb{1}_n\omega^d) + P^{\text{net}} + u - \nabla U(\delta).\end{aligned} \tag{II.4}$$

Observe that

$$\frac{dU(\delta)}{dt} = \nabla U^\top(\delta)\omega = \nabla U^\top(\delta)(I+\mu)^{-1}\bar{\omega}, \tag{II.5}$$

and that due to symmetry of the power flows P_i,

$$\mathbb{1}_n^\top \nabla U(\delta) = 0. \tag{II.6}$$

C. Generalized Averaging Integral Secondary control

In general, P^{net} in (II.4) is non-zero because the loads $G_{ii}V_i^2$ are usually unknown. Moreover, if the overall power balance is non-zero, then the steady state frequencies of the droop controlled MG (II.4) deviate from the nominal value ω^d. This steady state frequency error should be brought to zero using a secondary control law. In this paper, we focus on distributed secondary frequency control. Note that usually the internal frequency $\bar{\omega}_i$ is employed in distributed secondary frequency control [6], [12], [13], [10]. At first glance, this has the advantage that no additional frequency measurement is needed. However, it has been shown in [1] that the, generally unavoidable, presence of clock drifts also leads to non-negligible stationary frequency deviations when using any of the aforementioned control schemes. Motivated by this, we have proposed the following *generalized* distributed averaging integral (GDAI) secondary frequency control in [1]

$$\begin{aligned}u &= p,\\ (I_n + \mu)\dot{p} &= -\left((\mathbf{B} + \mathbf{C}\mathcal{L}_C)(\bar{\omega} - \mathbb{1}_n\omega^d) + \mathbf{D}\mathcal{L}_C p\right),\end{aligned} \tag{II.7}$$

where $\mathbf{B} \in \mathbb{R}^{n\times n}$, $\mathbf{C} \in \mathbb{R}^{n\times n}$ and $\mathbf{D} \in \mathbb{R}^{n\times n}$ are diagonal controller matrices and the symmetric positive semi-definite matrix $\mathcal{L}_\mathcal{C}$ is the Laplacian matrix representing the communication network.

For the subsequent analysis, it is convenient to introduce the notion below.

Definition 2.1: The closed loop system (II.4), (II.7) admits a synchronized motion if it has a solution for all $t \geq 0$ of the form

$$\delta^s(t) = \delta_0^s + \omega^s t, \quad \omega^s = \omega^*\mathbb{1}_n,$$

where $\omega^* \in \mathbb{R}$ is the synchronized electrical frequency and $\delta_0^s \in \mathbb{R}^n$ such that

$$|\delta_{0,i}^s - \delta_{0,k}^s| < \frac{\pi}{2} \quad \forall i \in \mathcal{N},\ \forall k \in \mathcal{N}_i.$$

The expression for ω^* is given by [1]

$$\omega^* = \frac{\mathbb{1}_n^T\mathbf{D}^{-1}\mathbf{B}\mathbb{1}_n}{\mathbb{1}_n^T\mathbf{D}^{-1}(\mathbf{B} + \mathbf{C}\mathcal{L}_\mathcal{C})(I_n+\mu)\mathbb{1}_n}\omega^d. \tag{II.8}$$

The matrix $\mathbf{B}$ is commonly called the *pinning gain matrix*, e.g. [6]. In the following, we define the clock of one of the units in the network as master clock, say the k-th unit, $k \geq 1$. Then, $\mu_k = 0$ and the drifts $\mu_i, i \neq k$ of all other clocks in the MG are expressed with respect to the master clock at k-th unit. In this scenario, it has been shown in [1] that selecting

$$\mathbf{B}\mu = \mathbb{0}_{n\times n}, \quad \mathbf{C} = -\mathbf{D}, \tag{II.9}$$

in (II.7) guarantees that $\omega^* = \omega^d$ in (II.8) together with active power sharing [5], [1] in the presence of clock drifts. Achieving both of these control objectives is, in general, not possible with [6] and the standard DAI control [12], [13], [10] in the presence of clock drifts, see [1] for more details.

D. Closed-Loop System

Combining (II.4) with (II.7) and using (II.9) yields the closed-loop dynamics

$$\begin{aligned}(I_n + \mu)\dot{\delta} &= \bar{\omega},\\ (I_n + \mu)M\dot{\bar{\omega}} &= -D(\bar{\omega} - \mathbb{1}_n\omega^d) - \nabla U(\delta) + P^{\text{net}} + p,\\ (I_n + \mu)\dot{p} &= -(\mathbf{B} - \mathbf{D}\mathcal{L}_C)(\bar{\omega} - \mathbb{1}_n\omega^d) - \mathbf{D}\mathcal{L}_C p.\end{aligned} \tag{II.10}$$

III. Robust GDAI Control Design

In this section, a tuning criterion is derived that ensures robust stability of the closed-loop MG dynamics (II.10) in the presence of clock drifts.

A. Error States and Problem Statement

We make the following standard assumption.

Assumption 3.1: The closed-loop system (II.10) possesses a synchronized motion. □

As the power flow equation (II.3) depends on the difference between angles, and not the angles itself, we follow [5], pick any arbitrary, say the n-th node and express all angles relative to that node. This coordinate reduction is given by

$$\theta = \mathcal{R}^\top\delta, \quad \theta \in \mathbb{R}^{n-1}, \quad \mathcal{R} = \begin{bmatrix} I_{n-1} \\ -\mathbb{1}_{n-1}^\top \end{bmatrix}. \tag{III.1}$$

Then, with Assumption 3.1, we introduce the error states

$$\begin{aligned}\tilde{\omega} &= \bar{\omega} - \bar{\omega}^* = \bar{\omega} - (I_n + \mu)^{-1}\mathbb{1}_n\omega^d,\\ \tilde{\theta} &= \theta - \theta^*, \quad \tilde{p} = p - p^*, \quad x = \text{col}\left(\tilde{\theta},\, \tilde{\omega},\, \tilde{p}\right).\end{aligned}$$

The resulting error dynamics of the system (II.10) is given by

$$\begin{aligned}\dot{\tilde{\theta}} &= \mathcal{R}^\top(I_n + \mu)^{-1}\tilde{\omega},\\ (I_n + \mu)M\dot{\tilde{\omega}} &= -D\tilde{\omega} - \mathcal{R}(\nabla U(\tilde{\theta} + \theta^*) - \nabla U(\theta^*)) + \tilde{p},\\ (I_n + \mu)\dot{\tilde{p}} &= (-\mathbf{B} + \mathbf{D}\mathcal{L}_C)\tilde{\omega} - \mathbf{D}\mathcal{L}_C\tilde{p},\end{aligned} \tag{III.2}$$

we define $x = \text{col}(\tilde{\theta}, \tilde{\omega}, \tilde{p}) \in \mathbb{R}^{3n-1}$ and $x^* = \mathbb{0}_{3n-1}$ is an equilibrium point of (III.2). Note that the asymptotic stability of $x^* = \mathbb{0}_{3n-1}$ implies asymptotic stability of the synchronized motion from Definition 2.1 in system (II.10) up to a uniform shift of all angles [5].

As outlined in [7], [9] for the purpose of secondary frequency control, it is reasonable to assume that the clock drifts are bounded. This is formalized in the assumption below.

Assumption 3.2: $\|\mu\|_2 \leq \epsilon, \quad 0 \leq \epsilon < 1.$

We are interested in the following problem.

Problem 3.3: Consider the system (III.2) with Assumption 3.1. Determine the matrices $\mathbf{B}$, $\mathbf{D}$ and $\mathcal{L}_C$, such that x^* is asymptotically stable for all μ satisfying Assumption 3.2.

B. Main result

For the presentation of our main result, it is convenient to define the matrices

$$\begin{aligned} T &= \begin{bmatrix} T_{11} & \frac{1}{2}\left(-I_n - \sigma \mathbf{D}^{-1}\mathbb{1}_n\mathbb{1}_n^\top D + \tilde{\mathbf{B}} - \mathcal{L}_{\mathcal{C}}\right) \\ * & T_{22} \end{bmatrix}, \\ \hat{T}_2 &= \begin{bmatrix} \sigma M\mathbb{1}_n\mathbb{1}_n^\top\tilde{\mathbf{B}} & \sigma\mathbf{D}^{-1}\mathbb{1}_n\mathbb{1}_n^\top D \\ \mathbb{0}_{n\times n} & -\sigma\mathbf{D}^{-1}\mathbb{1}_n\mathbb{1}_n^\top \end{bmatrix}, \end{aligned} \tag{III.3}$$

with $\sigma > 0$, $\tilde{\mathbf{B}} = \mathbf{D}^{-1}\mathbf{B} \geq 0$ and

$$\begin{aligned} T_{11} &= D - \frac{\sigma}{2}\left(M\mathbb{1}_n\mathbb{1}_n^\top\tilde{\mathbf{B}} + \tilde{\mathbf{B}}\mathbb{1}_n\mathbb{1}_n^\top M\right), \\ T_{22} &= \mathcal{L}_{\mathcal{C}} + \frac{\sigma}{2}\left(\mathbf{D}^{-1}\mathbb{1}_n\mathbb{1}_n^\top + \mathbb{1}_n\mathbb{1}_n^\top\mathbf{D}^{-1}\right). \end{aligned}$$

Furthermore, since μ is a diagonal matrix, with Assumption 3.2 we have that

$$\begin{aligned} \|\mu(I_n+\mu)^{-1}\|_2 \leq g_1(\epsilon), \quad g_1(\epsilon) = \tfrac{\epsilon}{1-\epsilon} > 0, \\ \|(\mu^2+2\mu)(I_n+\mu)^{-2}\|_2 \leq g_2(\epsilon), \quad g_2(\epsilon) = \tfrac{\epsilon^2+2\epsilon}{(1-\epsilon)^2} > 0. \end{aligned} \tag{III.4}$$

Our main result is as follows.

Proposition 3.4: Consider the system (III.2) with Assumption 3.1. Recall $g_1(\epsilon)$ and $g_2(\epsilon)$ defined in (III.4). Suppose that there exist $\sigma > 0$, $\zeta > 0$ such that

$$H_{\text{nom}} = \begin{bmatrix} M & -\sigma M\mathbb{1}_n\mathbb{1}_n^\top\mathbf{D}^{-1} \\ * & \mathbf{D}^{-1} \end{bmatrix} > \begin{bmatrix} g_2(\epsilon)M & \mathbb{0}_{n\times n} \\ \mathbb{0}_{n\times n} & g_1(\epsilon)\mathbf{D}^{-1} \end{bmatrix}, \tag{III.5}$$

and

$$\begin{aligned} T &> \left(\epsilon\zeta + g_1(\epsilon)\sqrt{\lambda_{\max}(D^2)+1}\right) I_{2n}, \\ 0 &\geq \begin{bmatrix} -\zeta I_{2n} & \hat{T}_2 \\ * & -\zeta I_{2n} \end{bmatrix}, \end{aligned} \tag{III.6}$$

where T and $\hat{T}_2$ are defined in (III.3). Then $x^* = \mathbb{0}_{3n-1}$ is a locally AS equilibrium point of the system (III.2) for all unknown clock drift factors satisfying Assumption 3.2.

Proof: Consider the Lyapunov function candidate

$$\begin{aligned} V = &\frac{1}{2}\tilde{\omega}^\top M\tilde{\omega} + U(\tilde{\theta}+\theta^*) - \nabla U(\theta^*)^\top\tilde{\theta} \\ &+ \frac{1}{2}\tilde{p}^\top\mathbf{D}^{-1}(I_n+\mu)\tilde{p} \\ &- \sigma\tilde{p}^\top(I_n+\mu)\mathbf{D}^{-1}\mathbb{1}_n\mathbb{1}_n^\top M(I_n+\mu)\tilde{\omega}, \end{aligned} \tag{III.7}$$

where $\sigma > 0$ is a design parameter. The Lyapunov function V contains kinetic and potential energy terms $\tilde{\omega}^\top M\tilde{\omega}$, respectively $U(\tilde{\theta})$ [21], a quadratic term in secondary control input $\tilde{p}$ and a cross term between $\tilde{\omega}$ and $\tilde{p}$ which allows us to ensure that V is decreasing along the trajectories of (III.2).

First, we will show that V is indeed positive definite. Note that

$$\nabla V\big|_{x^*} = \mathbb{0}_{3n-1}.$$

This shows that x^* is a critical point of V. Moreover, the Hessian of V evaluated at x^* is given by

$$\nabla^2 V|_{x*} = \begin{bmatrix} \nabla^2 U(\theta^*) & \mathbb{0}_{(n-1)\times n} & \mathbb{0}_{(n-1)\times n} \\ * & M & \nabla^2 V|_{(2,3)} \\ * & * & \mathbf{D}^{-1}(I_n+\mu) \end{bmatrix}, \tag{III.8}$$

with $\nabla^2 V|_{(2,3)} = -\sigma(I_n+\mu)M\mathbb{1}_n\mathbb{1}_n^\top\mathbf{D}^{-1}(I_n+\mu)$. Note that the matrix $\nabla^2 U(\theta^*) > 0$ [5]. Therefore, the Hessian $\nabla^2 V|_{x*}$ is positive definite if and only if

$$\begin{bmatrix} M & -\sigma(I_n+\mu)M\mathbb{1}_n\mathbb{1}_n^\top\mathbf{D}^{-1}(I_n+\mu) \\ * & \mathbf{D}^{-1}(I_n+\mu) \end{bmatrix} > 0. \tag{III.9}$$

By performing a congruence transformation using the positive definite matrix $S = \text{blkdiag}\left((I_n+\mu)^{-1}, (I_n+\mu)^{-1}\right)$ and by invoking Sylvester's law of inertia [22], we see that the matrix on the left hand side of (III.9) is positive definite if and only if the following matrix inequality is satisfied

$$\begin{bmatrix} (I_n+\mu)^{-2}M & -\sigma M\mathbb{1}_n\mathbb{1}_n^\top\mathbf{D}^{-1} \\ * & (I_n+\mu)^{-1}\mathbf{D}^{-1} \end{bmatrix} > 0. \tag{III.10}$$

The inequality (III.10) can be written as

$$H_{\text{nom}} - \begin{bmatrix} (\mu^2+2\mu)(I_n+\mu)^{-2}M & \mathbb{0}_{n\times n} \\ \mathbb{0}_{n\times n} & \mu(I_n+\mu)^{-1}\mathbf{D}^{-1} \end{bmatrix} > 0,$$

where H_{nom} is defined in (III.5). Furthermore, since μ, M and $\mathbf{D}$ are all diagonal matrices, we have that

$$\begin{bmatrix} (\mu^2+2\mu)(I_n+\mu)^{-2}M & \mathbb{0}_{n\times n} \\ \mathbb{0}_{n\times n} & \mu(I_n+\mu)^{-1}\mathbf{D}^{-1} \end{bmatrix} \leq \begin{bmatrix} g_2(\epsilon)M & \mathbb{0}_{n\times n} \\ \mathbb{0}_{n\times n} & g_1(\epsilon)\mathbf{D}^{-1} \end{bmatrix},$$

where $g_1(\epsilon)$ and $g_2(\epsilon)$ are defined in (III.4). Consequently, under the standing assumptions, see (III.5), $\nabla^2 V|_{x*} > 0$, confirming the positive definiteness of V. Note that $\nabla V\big|_{x^*} = \mathbb{0}_{3n-1}$ and $\nabla^2 V|_{x*} > 0$ implies that x^* is a strict local minimum of V [23].

Next, we calculate the time derivative of V along the solutions of (III.2), which yields

$$\begin{aligned} \dot{V} = &-\tilde{\omega}^\top(I_n+\mu)^{-1}D\tilde{\omega} + \tilde{\omega}^\top(I_n+\mu)^{-1}\tilde{p} \\ &+ \sigma\tilde{p}^\top(I_n+\mu)\mathbf{D}^{-1}\mathbb{1}_n\mathbb{1}_n^\top D\tilde{\omega} \\ &- \sigma\tilde{p}^\top(I_n+\mu)\mathbf{D}^{-1}\mathbb{1}_n\mathbb{1}_n^\top\tilde{p} - \tilde{p}^\top\mathbf{D}^{-1}\mathbf{B}\tilde{\omega} \\ &+ \tilde{p}^\top\mathcal{L}_{\mathcal{C}}\tilde{\omega} - \tilde{p}^\top\mathcal{L}_{\mathcal{C}}\tilde{p} + \sigma\tilde{\omega}^\top(I_n+\mu)M\mathbb{1}_n\mathbb{1}_n^\top\mathbf{D}^{-1}\mathbf{B}\tilde{\omega}, \\ = &-\eta^\top\begin{bmatrix} \mathbf{T}_{11} & \mathbf{T}_{12} \\ * & \mathbf{T}_{22} \end{bmatrix}\eta = -\eta^\top\mathbf{T}\eta, \end{aligned} \tag{III.11}$$

where $\eta = \text{col}(\tilde{\omega}, \tilde{p})$ and

$$\begin{aligned} \mathbf{T}_{11} &= (I_n+\mu)^{-1}D \\ &\quad - \tfrac{\sigma}{2}\left((I_n+\mu)M\mathbb{1}_n\mathbb{1}_n^\top\mathbf{D}^{-1}\mathbf{B} + \mathbf{D}^{-1}\mathbf{B}\mathbb{1}_n\mathbb{1}_n^\top M(I_n+\mu)\right), \\ \mathbf{T}_{22} &= \mathcal{L}_{\mathcal{C}} + \tfrac{\sigma}{2}\left((I_n+\mu)\mathbf{D}^{-1}\mathbb{1}_n\mathbb{1}_n^\top + \mathbb{1}_n\mathbb{1}_n^\top\mathbf{D}^{-1}(I_n+\mu)\right), \\ \mathbf{T}_{12} &= \frac{1}{2}\left(-(I_n+\mu)^{-1} - \sigma(I_n+\mu)\mathbf{D}^{-1}\mathbb{1}_n\mathbb{1}_n^\top D\right) \\ &\quad + \frac{1}{2}\left(\mathbf{D}^{-1}\mathbf{B} - \mathcal{L}_{\mathcal{C}}\right). \end{aligned}$$

Note that the entries of the matrix $\mathbf{T}$ in (III.11) are uncertain, because the clock drift matrix μ is uncertain. Hence, to obtain verifiable conditions that ensure $\mathbf{T} > 0$ and, thus, $\dot{V}(\eta)$ is negative definite, we note that $\mathbf{T}$ can be decomposed as

$$\mathbf{T} = T - \frac{1}{2}\left(\Gamma_1\hat{T}_1 + \hat{T}_1^\top\Gamma_1\right) - \frac{1}{2}\left(\Gamma_2\hat{T}_2 + \hat{T}_2^\top\Gamma_2\right), \tag{III.12}$$

where $\hat{T}_2$ is defined in (III.3) and

$$\begin{aligned}\hat{T}_1 &= \begin{bmatrix} D & -I_n \\ \mathbb{0}_{n\times n} & \mathbb{0}_{n\times n}\end{bmatrix},\\ \Gamma_1 &= \text{blkdiag}\left(\mu(I_n+\mu)^{-1}, \mu(I_n+\mu)^{-1}\right),\\ \Gamma_2 &= \text{blkdiag}\left(\mu, \mu\right).\end{aligned} \tag{III.13}$$

For any matrices $A \in \mathbb{R}^{n\times n}$ and $B \in \mathbb{R}^{n\times n}$, it holds that

$$AB + B^\top A^\top \leq 2\|A\|_2\|B\|_2 I_n.$$

Therefore from (III.12), we have that

$$\mathbf{T} \geq T - \left(\|\hat{T}_1\|_2\|\Gamma_1\|_2 + \|\hat{T}_2\|_2\|\Gamma_2\|_2\right) I_{2n}.$$

Assumption 3.2 together with (III.4), implies that

$$\|\Gamma_1\|_2 \leq g_1(\epsilon), \quad \|\Gamma_2\|_2 \leq \epsilon, \tag{III.14}$$

where Γ_1 and Γ_2 are defined in (III.13). Therefore,

$$\mathbf{T} \geq T - \left(g_1(\epsilon)\|\hat{T}_1\|_2 + \epsilon\|\hat{T}_2\|_2\right) I_{2n}. \tag{III.15}$$

From (III.13), we have that

$$\|\hat{T}_1\|_2 = \sqrt{\lambda_{\max}(\hat{T}_1\hat{T}_1^\top)} = \sqrt{\lambda_{\max}(D^2)+1}.$$

Turning to $\hat{T}_2$,

$$\begin{aligned} & \|\hat{T}_2\|_2 = \sqrt{\lambda_{\max}(\hat{T}_2\hat{T}_2^\top)} \leq \zeta,\\ \Leftrightarrow\ & \lambda_{\max}(\hat{T}_2\hat{T}_2^\top) \leq \zeta^2,\\ \Leftrightarrow\ & \hat{T}_2\hat{T}_2^\top \leq \zeta^2 I_{2n},\\ \Leftrightarrow\ & \frac{1}{\zeta}\hat{T}_2\hat{T}_2^\top - \zeta I_{2n} \leq 0,\end{aligned}$$

where $\zeta > 0$ is an upper bound for $\|\hat{T}_2\|_2$. By using the Schur complement [22], the last inequality above is equivalent to the second inequality in (III.6). Thus, from (III.15) we see that $\mathbf{T} > 0$ if

$$T - \left(\epsilon\zeta + g_1(\epsilon)\sqrt{\lambda_{\max}(D^2)+1}\right) I_{2n} > 0.$$

This is the first condition in (III.6). Thus, with the made assumptions, $\mathbf{T} > 0$ implies that

$$\begin{aligned}\dot{V}(\eta) &< 0 \quad \text{for} \quad \eta(t) \neq \mathbb{0}_{2n},\\ \dot{V}(\eta) &= 0 \quad \text{for} \quad \eta(t) = \mathbb{0}_{2n}.\end{aligned} \tag{III.16}$$

This shows that x^* is stable. Recall $\eta(t) = \text{col}(\tilde{\omega}, \tilde{p})$ and therefore $\dot{V}(\eta)$ does not depend on $\tilde{\theta}$.

Therefore, to conclude local asymptotic stability of x^*, we need to show that the following implication holds along solutions of the system (III.2)

$$\mathbf{T}\eta(t) \equiv \mathbb{0}_{2n} \quad \Rightarrow \quad \lim_{t\to\infty} x(t) = x^*. \tag{III.17}$$

Since $\mathbf{T} > 0$, from the second equation in (III.16), we have that

$$\tilde{\omega} = \mathbb{0}_n, \quad \tilde{p} = \mathbb{0}_n, \tag{III.18}$$

which, from (III.2), also implies that $\tilde{\theta}$ is constant. Moreover at $\eta(t) = \mathbb{0}_{2n}$, from the second equation in (III.2), we obtain that

$$\mathbb{0}_n = -\mathcal{R}(\nabla U(\tilde{\theta} + \theta^*) - \nabla U(\theta^*)), \tag{III.19}$$

which by multiplying from the left with $\mathcal{R}^\top$ and rearranging terms is equivalent to

$$\mathcal{R}^\top\mathcal{R}\nabla U(\tilde{\theta} + \theta^*) = \mathcal{R}^\top\mathcal{R}\nabla U(\theta^*). \tag{III.20}$$

Note that $\mathcal{R}^\top\mathcal{R}$ is invertible and recall that $\nabla^2 U(\theta^*) > 0$ [5]. Therefore, in a neighborhood of the origin, (III.20) only holds for $\tilde{\theta} = \mathbb{0}_{n-1}$. This shows that the implication (III.17) holds and hence that x^* is an AS equilibrium point, completing the proof. ■

Remark 3.5: By fixing the tuning parameter σ, the design conditions (III.5) and (III.6) are a set of LMIs that can be solved numerically efficiently using standard software [24]. Furthermore, the design conditions are independent of an actual equilibrium point. Consequently, if they are satisfied, then the corresponding GDAI controller guarantees local AS of any synchronized motion of the closed-loop dynamics (III.2).

IV. Case study

In this section, the performance and robustness of a MG operated with the control (II.7) designed via the criterion (III.5),(III.6) is illustrated. At first, we introduce the employed MG and then the simulation scenario.

The MG (Figure 1) used in the case study is simulated using MATLAB®/Simulink® and PLECS [25]. Constant impedance loads are connected at all GFIs. The system parameters are given in Table I. In order to evaluate the robustness of (III.5),(III.6) with respect to further model uncertainties, a small positive line resistance value is considered in the simulations, see Table I. Based on [7], [8], [26], the clock drift factors for the simulated GFIs are chosen as $\mu_1 = 0$, $\mu_2 = 1\text{ms}$, $\mu_3 = 0.5\text{ms}$ and $\mu_4 = -1\text{ms}$. Thus, the clock of GFI1 in Figure 1 is chosen as master clock and $\mathbf{B}$ is selected, such that $\mathbf{B}\mu = \mathbb{0}_{4\times 4}$ in (II.9). In the present case, this implies that $\mathbf{D}^{-1}\mathbf{B} = \tilde{\mathbf{B}} = \text{diag}(\tilde{b}, 0, 0, 0)$ where $\tilde{b} > 0$ is a design parameter. With the considered clock drift factors, $\epsilon = 0.001$ in Assumption 3.2.

The stability criterion (III.5), (III.6) is solved for $\mathbf{D}^{-1} > 0$, $\tilde{\mathbf{B}} \geq 0$ and $\mathcal{L}_\mathcal{C} \geq 0$ with $\sigma = 0.05$ and $\zeta = 2$ using the optimization toolbox Yalmip [24] and the solver Mosek [27] in MATLAB®/Simulink®. We obtained the parameters $\mathbf{D} > 0$, $\mathbf{B} \geq 0$ and the off-diagonal entries of the weighted Laplacian matrix $\mathcal{L}_\mathcal{C} \geq 0$ (see communication topology used

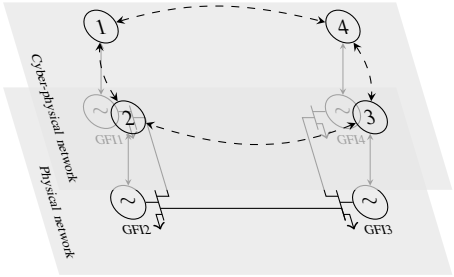

Fig. 1: MG used in simulation

TABLE I: MG parameters

Grid forming units		
Unit (at node)	M_i (MWs^2)	$D_i(MWs)$
GFI (1,2,3 and 4)	0.079	0.398
Constant impedance loads		
Unit (at node)	Apparent power [KVA]	Load power factor
Loads (1,2,3 and 4)	500	1
Line parameters		
Between nodes	Resistance [mΩ]	Inductance [μH]
1 and 2	0.71	20.2
2 and 3	3.5	101.2
3 and 4	2.8	80.9

in Figure 1) as

$$\mathbf{D} = \text{diag}(0.825, 1.174, 1.174, 1.174),$$
$$\mathbf{B} = \text{diag}(2.578, 0, 0, 0),$$
$$\mathcal{L}_{\mathcal{C}} = \begin{bmatrix} 2 & -0.667 & -0.667 & -0.667 \\ -0.667 & 2 & -0.667 & -0.667 \\ -0.667 & -0.667 & 2 & -0.667 \\ -0.667 & -0.667 & -0.667 & 2 \end{bmatrix}. \quad \text{(IV.1)}$$

The feasibility of (III.5), (III.6) implies that the equilibrium point of a GDAI controlled MG is locally AS in the presence of clock drifts. Furthermore, we simulate the GDAI controlled MG shown in Figure 1 using the parameters (IV.1). In simulation, power sharing weights [5], [1] were chosen as $\chi = D$ where $\mathcal{X} = \text{diag}(\mathcal{X}_i), \quad \mathcal{X}_i \in \mathbb{R}_{>0}$. The GDAI controller is activated at 10 seconds. In Figure 2, we can see that within a few seconds the *internal* inverter frequencies converge close to the nominal value ($\omega^d = 50$Hz), but not exatly to 50Hz in the presence of clock drifts. It has been shown in [1] that the aforementioned problem is noticeable even for usual distributed secondary frequency control schemes like [6], [12], [13], [10].

At first, we are interested in achieving $\omega^* = \omega^d$ using GDAI control (II.7), where ω^* is defined in (II.8). In the enlarged plot at 42.5 seconds in Figure 2, we can see that the synchronized electrical frequency ω^* (GFI1 frequency, green colored curve) coincides with $\omega^d = 50$Hz and hence confirms that $\omega^* = \omega^d$ at steady state. Furthermore, between 0 to 10 seconds, the weighted power flows given by $(P_i - P_i^d)/\mathcal{X}_i, i \in \mathcal{N}$ do not reach consensus. At 10 seconds, when the GDAI controller is activated, the weighted power flows attain consensus at steady state, see the enlarged plot for weighted power flows at 42.5 seconds. At 50 and 75 seconds, a constant power load of 500 kVA with unity power factor is added at GFI4 and GFI3 respectively. The control performance following the additional load steps at 50, respectively, 75 seconds is also satisfactory.

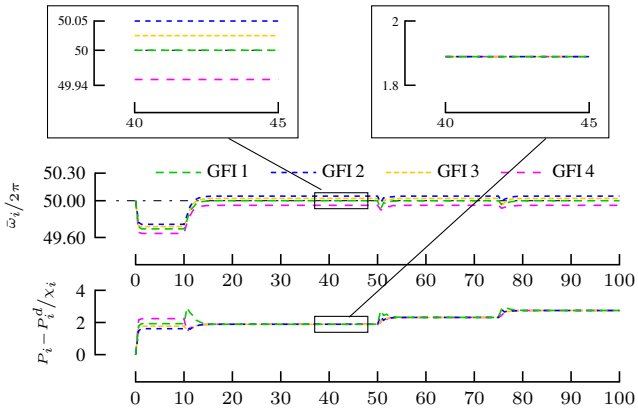

Fig. 2: Frequency ($\omega_i/2\pi$) and weighted power flows $(P_i - P_i^d)/\mathcal{X}_i$ versus time (in seconds)

V. Conclusions

A design criterion for a GDAI controlled MG ensuring robust stability in the presence of clock drifts is presented. We work with a non-linear MG model and hence there is no need for linearization to derive the design criterion. Unlike existing solutions for secondary frequency control in MGs, GDAI control achieves accurate steady state frequency restoration, power sharing and local AS in the presence of clock drifts. Finally, numerical solution and simulated output confirms the accomplishment of the aforementioned control objectives.

Future research will incorporate time delays in communication network used in GDAI control. Also, we plan to test the GDAI controller on a real MG. Another interesting aspect is to consider time varying voltage amplitudes in the analysis. Furthermore, a joint distributed secondary frequency and voltage control is an interesting, yet challenging problem especially if we consider model uncertainties and communication constraints.

References

[1] A. Krishna, C. A. Hans, J. Schiffer, J. Raisch, and T. Kral, "Steady state evaluation of distributed secondary frequency control strategies for microgrids in the presence of clock drifts," in *25th Mediterranean Conference on Control and Automation (MED)*, 2017, pp. 508 – 515.

[2] J. Lopes, C. Moreira, and A. Madureira, "Defining control strategies for microgrids islanded operation," *IEEE Transactions on Power Systems*, vol. 21, no. 2, pp. 916 – 924, May 2006.

[3] J. Schiffer, D. Zonetti, R. Ortega, A. Stanković, J. Raisch, and T. Sezi, "Modeling of microgrids - from fundamental physics to phasors and voltage sources," *Automatica*, vol. 74, no. 12, pp. 135–150, 2016.

[4] J. Guerrero, P. Loh, M. Chandorkar, and T. Lee, "Advanced control architectures for intelligent microgrids – part I: Decentralized and hierarchical control," *IEEE Transactions on Industrial Electronics*, vol. 60, no. 4, pp. 1254–1262, 2013.

[5] J. Schiffer, R. Ortega, A. Astolfi, J. Raisch, and T. Sezi, "Conditions for stability of droop-controlled inverter-based microgrids," *Automatica*, vol. 50, no. 10, pp. 2457–2469, 2014.

[6] A. Bidram, F. Lewis, and A. Davoudi, "Distributed control systems for small-scale power networks: Using multiagent cooperative control theory," *IEEE Control Systems*, vol. 34, no. 6, pp. 56–77, 2014.

[7] J. Schiffer, C. A. Hans, T. Kral, R. Ortega, and J. Raisch, "Modeling, analysis, and experimental validation of clock drift effects in low-inertia power systems," *IEEE Transactions on Industrial Electronics*, vol. 64, pp. 5942 – 5951, 2017.

[8] Anritsu, "Understanding frequency accuracy in crystal controlled instruments - application note," Anritsu EMEA Ltd., Tech. Rep., 2001.

[9] J. Schiffer, R. Ortega, C. Hans, and J. Raisch, "Droop-controlled inverter-based microgrids are robust to clock drifts," *American Control Conference*, pp. 2341 – 2346, 2015.

[10] J. W. Simpson-Porco, Q. Shafiee, F. Dörfler, J. C. Vasquez, J. M. Guerrero, and F. Bullo, "Secondary frequency and voltage control of islanded microgrids via distributed averaging," *IEEE Transactions on Industrial Electronics*, vol. 62, pp. 7025–7038, 2015.

[11] J. Schiffer, F. Dörfler, and E. Fridman, "Robustness of distributed averaging control in power systems: Time delays & dynamic communication topology," *Automatica*, vol. 80, pp. 261–271, 2017.

[12] X. Fu, F. Dörfler, and M. R. Jovanović, "Topology identification and design of distributed integral action in power networks," in *American Control Conference (ACC)*, 2016, pp. 5921 – 5926.

[13] C. D. Persis, N. Monshizadeh, J. Schiffer, and F. Dörfler, "A lyapunov approach to control of microgrids with a network-preserved differential-algebraic model," in *IEEE 55th Conference on Decision and Control (CDC)*, 2016, pp. 2595 – 2600.

[14] R. R. Kolluri, I. Mareels, T. Alpcan, M. Brazil, J. de Hoog, and D. A. Thomas, "Power sharing in angle droop controlled microgrids," *IEEE Transactions on Power Systems*, 2017.

[15] C. D. Persis and N. Monshizadeh, "Bregman storage functions for microgrid control," *IEEE Transactions on Automatic Control*, 2017.

[16] C. Godsil and G. Royle, *Algebraic Graph Theory*. Springer, 2001.

[17] M. Mesbahi and M. Egerstedt, *Graph theoretic methods in multiagent networks*. Princeton University Press, 2010.

[18] P. Kundur, *Power system stability and control*. McGraw-Hill, 1994.

[19] J. W. Simpson-Porco, F. Dörfler, and F. Bullo, "Synchronization and power sharing for droop-controlled inverters in islanded microgrids," *Automatica*, vol. 49, no. 9, pp. 2603 – 2611, 2013.

[20] J. Schiffer, D. Goldin, J. Raisch, and T. Sezi, "Synchronization of droop-controlled microgrids with distributed rotational and electronic generation," in *52nd Conference on Decision and Control*, Florence, Italy, 2013, pp. 2334–2339.

[21] M. A. Pai, *Energy function analysis for power system stability*. Kluwer academic publishers, 1989.

[22] R. A. Horn and C. R. Johnson, *Matrix analysis*. Cambridge university press, 2012.

[23] A. van der Schaft, *L2-Gain and Passivity Techniques in Nonlinear Control*. Springer, 2000.

[24] J. Löfberg, "YALMIP : a toolbox for modeling and optimization in MATLAB," in *IEEE International Symposium on Computer Aided Control Systems Design*, sept. 2004, pp. 284 –289.

[25] Plexim GmbH, "Plecs software, www.plexim.com," 2013.

[26] *Schneider Electric, Conext XW inverter/charger product manual, 2014, [Online; accessed 8-November-2014]. [Online]. Available: http://www.schneider-electric.com/products/au*.

[27] Mosek, "The mosek optimization toolbox, www.mosek.com."